



TECHNICAL ARTICLE

Experimental Investigation and Prediction of Mild Steel Turning Performances Using Hybrid Deep Convolutional Neural Network-Based Manta-Ray Foraging Optimizer

Thangavel Palaniappan and Prakasam Subramaniam

Submitted: 26 April 2021 / Revised: 23 November 2021 / Accepted: 2 December 2021 / Published online: 14 January 2022

In machining industries, sustainable production activities are reduced because of the tool wear effect. The machining input parameters are mainly responsible for the effect of flank wear attained in the tool and the workpiece's surface quality. This work aims to determine and predict the machining performances of EN2-BS970/Mild steel by varying the input parameters such as cutting speed (V), feed (F), nose radius (r), and depth of cut (d). The hybrid Deep Convolutional Neural Network-based Manta-Ray Optimization (DCNN-MRO) is used to predict the machining outcomes, and it is performed in Matlab software version 2020a. The input machining parameters are designed by response surface methodology of box behnken design performed in Design-Expert software version 11. The experimented different cutting forces are feed force (F_x), radial force (F_y), cutting force (F_z), and the machining performances are tool flank wear, surface roughness, and Tool chip thickness. In which, the machining input parameter, namely cutting speed effectively influences the turning outcomes. The effect of tool flank wear and surface roughness by varying the cutting forces are also analyzed. The observed optimal surface roughness is $3.105 \mu\text{m}$, tool wear rate is 0.139mm , and tool chip thickness is 0.11mm . The measured outcomes are closer to the predicted outcomes obtained from hybrid DCNN. The average RMSE obtained from the proposed DCNN-MRFO is 0.03, and the non-hybrid DCNN is 0.3.

Keywords convolutional neural network, Manta-Ray optimization, mild steel, surface roughness, turning operation

1. Introduction

Nowadays, modern industries face superior challenges to achieve a better surface finish, high dimensional accuracy, minimal wear, enhanced productivity, etc. In manufacturing technology, the machining process is considered a common and leading approach. The manufacturing and maintenance costs are maximized during metal cutting operations due to tool wear and surface roughness rate. This is because of surface roughness and tool wear which is directly involved in suppressing the work piece's quality, productivity limit, etc. (Ref 1). In lathe machining, turning is considered a superior operation, and it allows the workpiece to plastic deformation during machining. This effect promotes the formation of heat on the surface of the materials.

In some cases, this may reduce the workpiece's mechanical behavior, namely fatigue strength and hardness (Ref 2). Mild steel is mainly used in aerospace applications, especially

welding and fitting of aerospace components. Besides, the deforming ability of Mild steel is more, and there is a chance for forming tool flank surface wear and generating built-up-edge (Ref 3). Normally, different tool materials such as steel, tungsten, and tungsten carbide are used in turning operations. Among them, tungsten carbide possesses better toughness, resistance to impact, and is wear-resistant during machining. Several researchers have focused on using the insert tool rather than the solid tool for the turning operation in the lathe. This is because of its higher cutting efficiency, enhanced production rates. Rafighi et al. (Ref 4) conducted the machining of turning in High Chromium AISI D2 steel with the ceramic and cubic boron nitride (CBN) inserts with different nose radius. Surface roughness is favorable using CBN inserts, and minimal cutting forces are observed when using ceramic inserts. In another work, Rajaparathiban et al. (Ref 5) utilized a carbide insert for machining the EN 31 steel, and surface roughness is measured. In another work, the carbide insert was used to machine the AISI 1020 steel with the cryogenic application, in which gray relational analysis was conducted to predict the machining outcomes (Ref 6). AISI D6 alloy die steel was machined using nanoparticles coated carbide tool, and positive outcomes such as longer tool life and better surface finish were observed. Besides, more wear rate and minimum surface roughness was observed at the high cutting speed (Ref 7).

In the turning operation, the cutting force analysis is vital for studying the machining performances. Forces consideration is conveniently applicable for three components: radial, cutting, and feed (Ref 8). The speed, depth of cut, and feed promote cutting force are changes required for machining parameters. Thus, the accuracy of the machining process gets enhanced

Thangavel Palaniappan and Prakasam Subramaniam, Department of Mechanical Engineering, Shree Venkateshwara Hi-Tech Engineering College, Othakuthirai, Gobichettipalayam, Erode District, Tamil Nadu 638455, India. Contact e-mail: thangspro@gmail.com.

through several cutting force applications (Ref 9). During machining, the rubbing action is involved between the workpiece and tool flank side, maximizing the effect of tool wear. With the increasing feed rate and cutting force cutting velocity, the temperature attained in the chip forming region increases (Ref 10, 11). Many types of research are helping to study the cutting forces of lathe machining operations. However, the lathe machining of Mild steel is less contribute to force analysis. Ghuge and Mahalle (Ref 12) have been conducted experimentation to analyze the cutting forces while turning of AISI 4130. The finding revealed that by the MQL application, nearly 5 to 10% of cutting force gets suppressed.

Tool wear and surface roughness are important to enhance the product's quality and production and production process planning in the machining industry (Ref 13-15). The attained wear in the tool is an important factor for forecasting the tool life. Tool flank wear is often used as the specification to determine the precision and stability of machining. Flank wear (VB) occurs primarily during turning operations. In the machining process, the machining element's reliability depends on how much flank wear it is. It cannot be ignored because of its primary influence on surface integrity and dimensionally incorrectness (Ref 16). An increase in flank wear causes the inserts to decrease their nose radius and reduces surface quality (Ref 17). One way that the industry can reduce production costs is through the maximum use of the cutting tool. Hence, the tool wear must be controlled and kept within a limit for machining. Therefore, a precise method model should be developed to maximize the total economy by turning operations (Ref 18). Şahinoğlu, A., Rafiqhi, M (Ref 19) investigated the performances such as sound intensity, surface roughness, and vibration during AISI 4140 turning operation. In which the effect of feed rate was the most influencing factor for the entire performance.

In AISI 316 austenitic stainless steel, Atla, S. and Surya, M.S (Ref 20) have been measured the surface roughness and tool wear characteristics through turning. Authors proved that better performances and machining efficiency had been provided when using oil-based coolant than in the dry environment. Mia and Dhar (Ref 21) studied surface finishing of steel workpieces and found that surface finishing and interface temperatures were affected the product hardness. The increasing cutting speed resulted in the excellent finishing of the surface with a high-pressure coolant value. Recently, Şahinoğlu and Rafiqhi (Ref 22) proposed a research work to minimize surface roughness and power consumption of AISI 1040 steels. In this, the effect of machining inputs over output variables was determined using RSM. The result proved that feed rate negatively impacts the entire machine outcomes, such as power consumption, sound level, and surface roughness. Besides, the deep cryogenically treated tool and coolant are utilized by several researchers for machining the steel material.

In the lathe operation, Furgan Bayraktar and Fuat Kara (Ref 23) utilized a cryogenically treated cutting tool to analyze the surface roughness behavior of the Sleipner cold work steel. In which the untreated tool promotes more surface roughness. Das et al. (Ref 24) have been utilized the nanoparticles contributed MQL approach for machining the AISI 4340 alloy steel. Even though such cryogenic and MQL application promotes better machinability, it may be quite cost expensive. The optimization methods, namely Taguchi optimization, RSM method, are utilized to design and optimize the turning parameters (Ref 25). Fuat Kara (Ref 26) has been optimized the milling character-

istics using Taguchi L16 orthogonal array of Hardox 400 Steel, and the outcomes are optimized based on the S/N ratio. At cutting speed 120m/min, better surface roughness was obtained.

The machining performances such as dimensional accuracy and surface roughness of any lathe operation are predicted and optimized using RSM (Ref 27). Kishore and Rao (Ref 28) analyzed the influence of input parameters like speed, feed, and depth of cut on the output parameter of cutting force flank wear and surface roughness using Taguchi design for the design of experiments. Kuntoglu and Saglam (Ref 29) have been conducted the lathe turning operation on ALSI 1050 material with different input parameters, namely the tip of the tool, feed rate, and speed. The experimental plan was performed by Taguchi, and ANOVA approach is used to validate the machining performances. From the input turning parameters, cutting speed is significantly effective, and it was determined from ANOVA.D. Manivel and R. Gandhinathan (Ref 30) experimentally investigated the Tool wear and surface roughness of ductile iron by employing the Taguchi optimization method. Carbide insert was employed for hard turning operations, and cutting parameters were optimized based on the Taguchi method. Depth of cut, cutting speed, nose radius, and feed rate was taken as input parameters. It was evident that the surface roughness and tool wear are mostly influenced by cutting speed. Mozammel Mia et al. (Ref 31) investigated tool wear and material removal rate formed on Taguchi optimization in hard turning under MQL conditions. Tool wear, surface roughness, and material removal rate were optimized by Taguchi signal to noise. It has been found the depth of cut and feed rate of 1.5 mm and 0.2mm/rev, and cutting speed of 90m/min was responsible for maximum cutting rate and minimum surface roughness.

Various Neural network-based methods in the past have predicted the impact of the machining parameter. This technique is used to minimize the experimental program's time, cost, and accuracy, cross-examine the factor interaction and effect of individual factors, execution, and careful planning (Ref 32, 33). SK and Shankar (Ref 34) experimentally investigated the surface roughness and cutting force of EN8 steel by using an artificial neural network. 27.7% cutting depth strongly influenced the cutting force, and the cutting force was slightly influenced by cutting speed. 41.67% cutting depth and 21.33 % feed highly influenced the surface roughness. Salimi et al.(Ref 35) have been conducted the prediction analysis on cutting tool wear utilizing Artificial Neural Network (ANN) with the input parameters, namely cutting forces and vibration. Such prediction process is achieved with the regression value '1.' The accuracy of the mild steel turning performance is predicted by Sada (Ref 36) using ANN and proved that the experimented outcomes are highly significant to the predicted values with RMSE < 1.

Normally, in the existing works, the nose radius of the carbide tool is kept as 0.4mm, 0.8 mm, and 1.2 mm during turning operation. In this work, different nose radius values are used instead of standard nose radius, and the turning performances of mild steel are investigated. The contribution of neural networks is rare to predict machining performances. In our work, the hybrid Deep Recurrent Neural Network (DCNN)-based Manta-Ray Foraging Optimization is employed to forecast the experimented values. Besides, the proposed predicted outcomes are compared with the DCNN.

The main contributions of this work are listed below:

- To forecast the experimentally analyzed parameters of the workpiece during turning of mild steel, like cutting forces, flank wear of tool, tool chip thickness, and surface roughness.
- The lathe machining performances of the workpiece are analyzed to vary the input parameters, namely speed, nose radius, depth of cut, and feed.
- The hybrid Deep convolutional Neural network-based Manta-Ray Foraging Optimizer is used to forecast the machining performances and cutting forces.

2. Proposed Methodology

A study of feed, speed, and cutting depth has been extremely active on the lathe machining. Still, this research has continuously been needed for the various combinations of tools and workpieces. During monitoring the cutting conditions, the cutting forces are an important criterion to choose on output parameters, such as tool life, surface roughness, and tool wear. The Deep convolutional Neural network (DCNN) includes three cutting force components and tool flank wear (VB) to predict surface roughness. Therefore, the tool condition monitoring system produces a signal to ensure that the surface roughness is preserved in the desired range. In our work, the Tungsten carbide tool is used to machine the EN2-BS970/Mild steel-IS226 steel with different input of machining conditions such as speed (V), depth of cut (d), nose radius (r), and feed (F).

Figure 1 demonstrates the proposed procedure of our work as step by step manner. Initially, the feasibility analysis is carried out to select the best input machining condition of EN2-BS970/Mild steel-IS226 steel. The fixed machining input parameters are speed, depth of cut, nose radius, and feed. Box Behnken design is used to plan the experimental parameters and is performed using Design-Expert software. The experimentation is then carried out to determine the cutting forces, tool wear, surface roughness, tool chip thickness during machining. The hybrid DCNN-based Manta-Ray optimization is used to predict the experimented machining performances and cutting forces. The predicted outcomes obtained from the proposed hybrid approach are also compared with the non-hybrid Deep Convolutional Neural network-based prediction.

3. Experimentation

In our work, the machining parameters' design is constructed by Response surface methodology with the help of Box Behnken Design and is performed in Design-Expert Software. Initially, a preliminary analysis is carried out to find the superior range of input parameters. In our work, the existing research papers majorly contribute to selecting the range of input parameters except for nose radius (Ref 4-29). Normally, the standard nose radius such as 0.4, 0.8, and 1.2 mm is used in the existing papers. In the proposed work, nose radius such as 0.5 mm, 0.75 mm, and 1 mm are chosen. The obtained turning performances for the selected range of nose radius are closer to the standard nose radius values. Finally, the desired machining performance was observed by conducting several experiments with different input ranges. The selected machining parameters levels are given in Table 1.

The model matrix chosen for the experiments was the Box Behnken design, consisting of 25 coded conditions. EN2-BS970/Mild steel-IS226 was machined using a carbide tool. The dimension of the workpiece is 150 mm in length and 30 mm in diameter. The Kistler dynamometer (type 9257B) is utilized to calculate the cutting force component and the three orthogonal components of feed force (F_x or F_f), radial force (F_y or F_r), and cutting force (F_z or F_t or F_c), were measured quasi-statically. Certain constant secondary parameters are used, namely tool height, tool geometry, tool overhang, and material hardness. The first end of the workpiece is connected in the chuck, and the second end remains uncontrolled. The chuck was housed the 150 mm lengthened workpiece. For this experiment, the turning of 30 mm on each specimen was repeated for three repetitions to evaluate the tool flank wear. The average VB width of the tool flank wear was measured by the microscope of the toolmaker (Metzer, model METZ -1395).

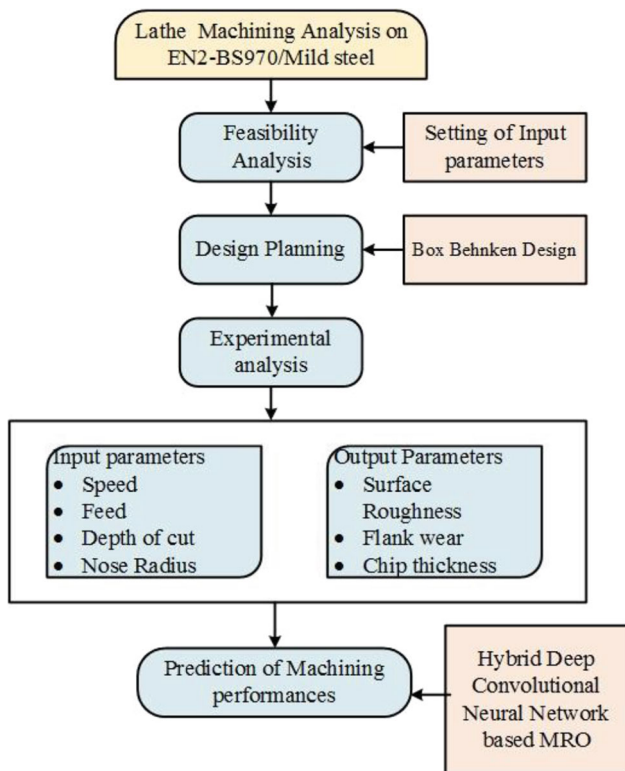


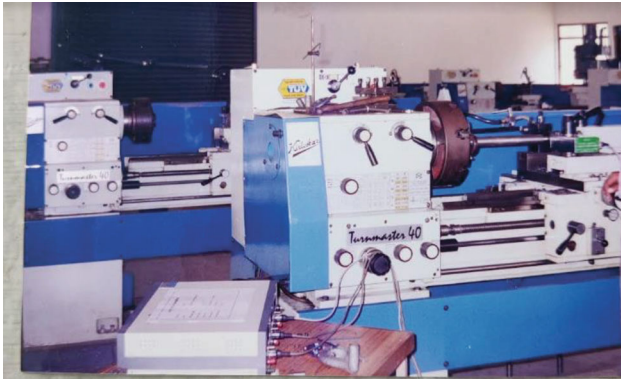
Fig. 1 Proposed scheme of research work

Table 1 Levels and Factors of machining parameters

Parameter	Factor Levels		
	1	2	3
Cutting speed (V), m/min	110	170	264
Feed rate (F), mm/rev	0.110	0.159	0.220
Depth of cut (d), mm	1.5	2.0	2.5
Nose Radius (r), mm	0.5	0.75	1

The lathe machining of mild steel and utilized workpieces are given in Fig. 2.

The workpieces' surface roughness (Ra) is measured using the SJ-400 Surftest Surface roughness tester with a cut-off length of 0.8 mm. Using the surface tester, Ra is measured periodically at three different places on the surface of the



(a) Machining setup



(b) EN2-BS970/Mild steel workpieces

Fig. 2 Lathe machining

specimen. Among these three measurements, the arithmetic mean value is taken to select the final roughness values. By varying the input variables, VB and Ra values were measured in 25 tests. The lathe machining layout is provided in Fig. 3. The specification of the lathe machining process is given Table 2.

3.1 Hybrid Deep Convolution Neural Network-Based Manta-Ray Foraging Optimization (DCNN-MRFO)

This work forecasted the machining performances using a hybrid Deep Convolutional Neural Network (DCNN)-based Manta-Ray Foraging optimization (MRFO). Two layers, namely, the pooling and convolutional layers, are the leading agents in DCNN (Ref 37) and are demonstrated in Fig. 4. Normally, in the neural network, random weights are selected to predict the desired performances. In our work, the optimization method, namely MRFO, is utilized to optimize the desired weight values and improve forecasting accuracy. The utilized DCNN parameters are specified in Table 3.

The outputs in the training stage are formed by bias addition with activation function, which is performed in the convolutional layer. In this work, three different activation functions, namely hyperbolic tangent (tanh), sigmoid, and Rectified Linear unit (ReLU) are utilized to predict the experimental outcomes. Such activation function helps provide the weighed output (Ref 38) and takes place between 0 and 1. To avoid the random weight updating process, Manta-Ray Foraging Optimizer is used to optimize the weight values. The normalization process helps to faster learning and minimizes the number of epochs. In this work, normalization is taking place in the entire dataset ranges from 0 to 1, to achieve the desired target. Besides, superior activation function to be determined based on the performance.

The outputs of the convolution layer are expressed below,

$$x_j^l = ac(z) \quad (\text{Eq 1})$$

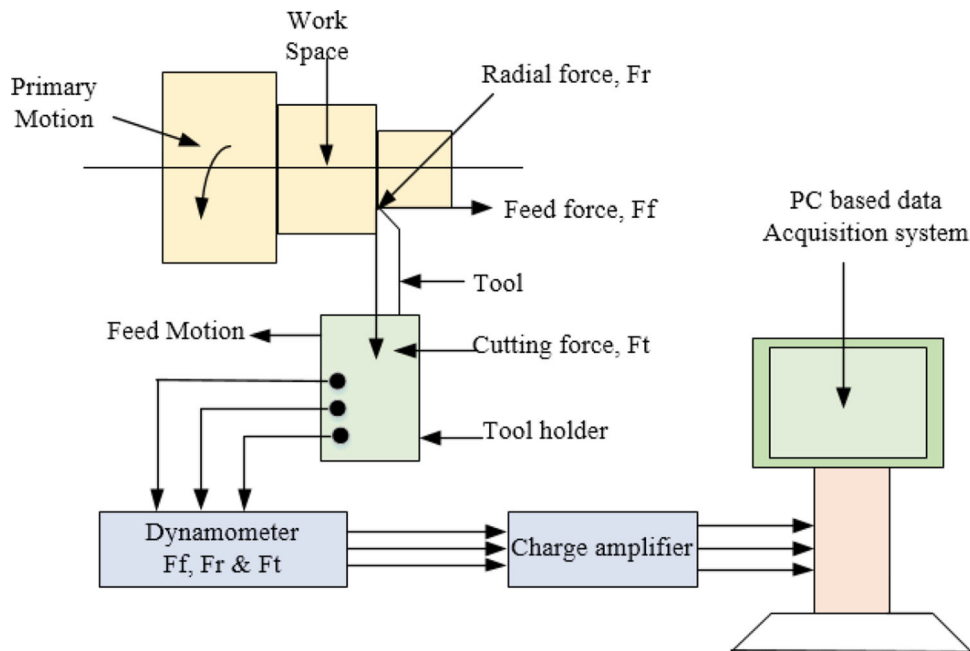


Fig. 3 Machining layout

Table 2 Machining condition used for the experimentation

Machine tool	Bharat machine tools, type 175
Cutting tool	Tungsten carbide (CNMG 1204 08.49), Rhombic insert, nose 80°
Tool Geometry	Tool size: 19mm X 19mm X90mm length. SR 9°, BR 9°, ER 6°, ECEA 7°, SRF 7°, Nose: 0.75 mm
Workpiece dimension	30 mm diameter with 150 mm length
Work Material	EN24 Steel
Cutting Fluid	Dry Condition

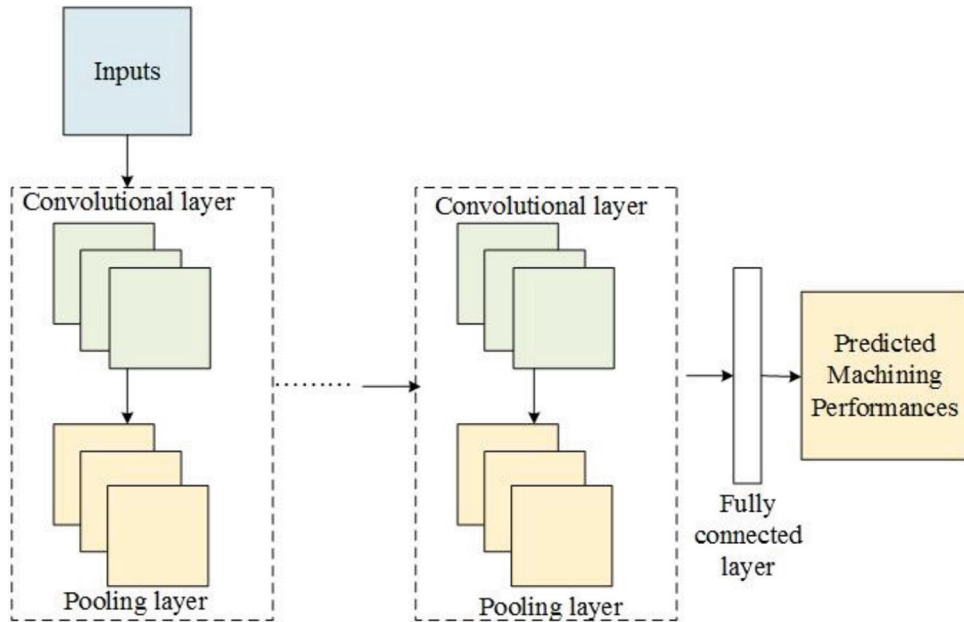


Fig. 4 Layout of deep convolutional neural network

Table 3 DCNN parameters during prediction

No. Of Convolution layer	2
No. of Pooling layer	2
No. of fully connected layer	1
Average training time	98 sec
Size of pooling layer	1x2
Size of convolution filter (layer 1)	27x4
Size of convolution filter (layer 2)	1x3
Learning rate	0.01
Epochs	35

Layers	Weight parameters	Bias parameters
Convolution layer 1	155	25
Convolution layer 2	320	54
Pooling layer	0	0
Fixed layer	10550	110
Total	11214	

$$\tanh(z) = \frac{e^z - e^{-z}}{e^z + e^{-z}}$$

(Eq 2)

$$ReLU(z) = \max(z, 0)$$

(Eq 4)

$$\text{sigmoid}(z) = \frac{1}{1 + e^{-z}}$$

(Eq 3)

$$z = \sum_i x_i^{l-1} * w_{ij}^{l-1} + b_j^l$$

(Eq 5)

Where, the convolutional output and input values are denoted as x_j^l and x_i^{l-1} , the convolution operator is denoted as ‘*’,

Table 4 Machining characteristics

Test no	Speed (V), m/min	F, mm/rev	d, mm	R, mm	Ff, N	Fr, N	Fc, N	VB, mm	T _{ch} , mm	Ra, μm
1	264	0.110	2.5	0.5	82	142	215	0.292	0.28	3.758
2	264	0.220	1.5	1	264	367	527	0.295	0.32	3.865
3	170	0.159	2	0.75	69	106	185	0.249	0.256	3.891
4	110	0.220	2.5	0.5	72	109	193	0.303	0.338	3.256
5	264	0.110	2.5	1	278	327	533	0.324	0.352	3.758
6	264	0.220	2.5	0.5	145	276	401	0.329	0.363	4.917
7	170	0.159	2	0.75	71	109	188	0.251	0.263	3.458
8	110	0.220	2.5	1	116	169	228	0.279	0.283	3.279
9	110	0.110	2.5	1	111	160	221	0.139	0.11	3.105
10	110	0.110	1.5	1	79	107	196	0.172	0.153	5.211
11	170	0.159	2	0.75	69	102	183	0.248	0.251	4.958
12	264	0.110	1.5	0.5	81	117	203	0.296	0.274	4.765
13	110	0.220	1.5	0.5	78	97	195	0.231	0.259	3.389
14	110	0.110	1.5	0.5	67	82	187	0.159	0.133	3.896
15	170	0.159	2	0.75	73	109	191	0.250	0.273	4.801
16	110	0.159	2	0.75	67	127	168	0.211	0.241	4.396
17	264	0.159	2	0.75	113	192	278	0.253	0.25	3.268
18	170	0.110	2	0.75	102	156	278	0.146	0.177	3.763
19	170	0.220	2	0.75	210	251	401	0.306	0.364	3.356
20	170	0.110	2	0.75	74	101	193	0.248	0.262	3.758
21	170	0.110	1.5	0.75	112	215	249	0.225	0.251	3.760
22	170	0.110	2.5	0.75	93	144	208	0.229	0.269	3.751
23	170	0.110	2	0.5	70	105	187	0.220	0.251	4.459
24	170	0.110	2	1	121	141	289	0.228	0.259	3.756
25	170	0.110	2	0.75	76	113	197	0.236	0.277	3.765

sigm() represents the sigmoid function, and the non-linear sigmoid input function is represented as z_j^l . b_j^l and w_{ij}^{l-1} represents the bias and weight values. The filters size such as Dx4 and 1x3 are used for the first and second convolution layers.

The sub-sampling behavior of the input features is performed in the pooling layer. In this, the overlapping activity is not contributed to the average pooling approach. Here, the pooling filters are the size of 1x2. From the pooling layers, the obtained output features expressed below,

$$x_j^l = \text{down}(x_j^l) \tag{Eq 6}$$

In which, x_j^l and x_j^{l+1} represents the input and output of the pooling layer. During average pooling, the sub-sampling activity is denoted as *down(.)*.

The predicted outcomes are gained from the training stage through multilayer perceptron training, and this activity is performed after feature extraction. The Multilayer perceptron training is completely performed based on the squared error loss function.

$$E = \frac{1}{2}(y(t) - y^*(t))^2 \tag{Eq 7}$$

The squared error loss function is denoted as ‘E’, and the predicted and the target machining performances are denoted as $y(t)$ and $y^*(t)$.

Usually, in the neural network, the prediction process is achieved through a random weight-updating manner. Such activity is expressed in the following equation,

$$w_{ij}^l = w_{ij}^l - \eta \frac{\partial E}{\partial w_{ij}^l} \tag{Eq 8}$$

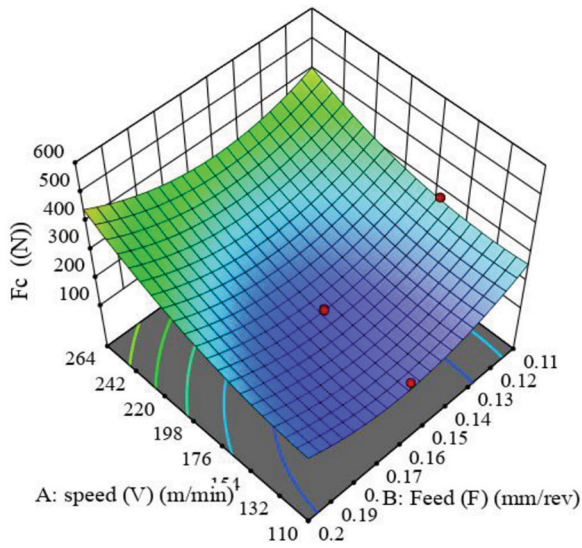
The learning rate in the training stage is denoted as η and the influence of weight values on the experimented values is defined. Certain alterations are required for the weights w_{ij} if the gained learning rate is not usual or too large w_{ij} . In addition to the random weight updating procedures, the MRFA based optimized weight values are also utilized to enhance the prediction performances. Such optimization procedures are explained below.

3.1.1 Manta-Ray Foraging Algorithm (MRFA). In the Manta-ray Foraging algorithm (MRFA), the manta-rays utilize three different strategies: chain-based foraging, cyclone foraging, and somersault-based foraging to select their suitable planktons (Ref 39). In our work, Manta-Rays foraging are considered weight values and used to determine the optimal minimal error values.

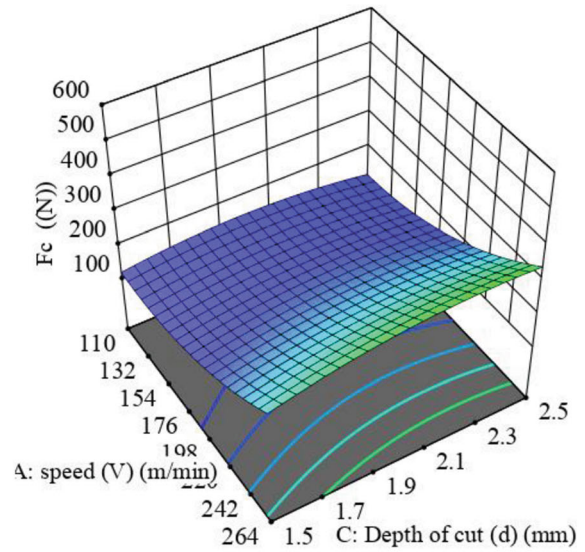
3.1.2 Chain Foraging. This is the initial foraging process, in which the weight values are assembled in the form of a chain to reach minimal error. The final weight values can determine the minimal error during chain action than proceedings (Ref 40). In this case, there is a chance of missing the selection of the best minimal error values. The end weight value from the chain selects a random value, which is not an optimal minimized error value. The mathematical model for this strategy is given below,

$$x_i^d(t+1) = \begin{cases} x_i^d + n(x_{best}^d(t) - x_i^d(t)) + b(x_{best}^d(t) - x_i^d(t)), & i = 1 \\ x_i^d(t) + n(x_{i-1}^d(t) + x_i^d(t)) + a(x_{best}^d(t) - x_i^d(t)), & i = 2, \dots, N \end{cases} \tag{Eq 9}$$

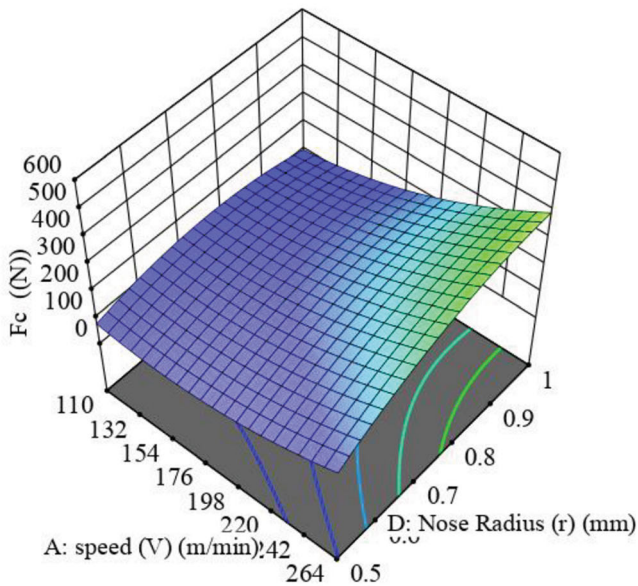
$$b = 2n\sqrt{|\log(n)|} \tag{Eq 10}$$



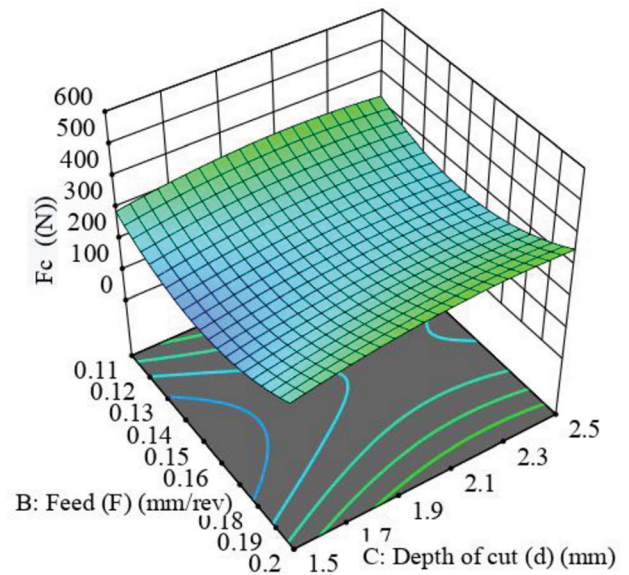
(a) Effect of Feed Rate and speed on F_c ($d=2$, $r=0.75$)



(b) Effect of Depth of cut and speed on F_c ($F=0.155$, $r=0.75$)



(c) Effect of Feed Rate and Nose Radius on F_c ($F=0.155$, $d=2$)



(d) Effect of Feed Rate and Depth of cut on F_c ($V=232$, $r=0.75$)

Fig. 5 3-D Surface analysis for analyzing the influence of input parameters on cutting forces

At time t , the location of the individual at dimension 'd' is represented as x_d^i , and the weight coefficient is expressed as 'b', 'n' represents the random number between [0,1], and the optimal error value is denoted as $x_{best}^d(t)$.

3.1.3 Cyclone Foraging. After the attainment of chain motion, the spiral movement is achieved by the entire weight values. The cyclone foraging strategy is given in the following equation,

$$x_i^d(t+1) = \begin{cases} x_{best}^d + n(x_{best}^d(t) - x_i^d(t)) + \alpha(x_{best}^d(t) - x_i^d(t)), & i = 1 \\ x_{best}^d(t) + n(x_{i-1}^d(t) + x_i^d(t)) + \alpha(x_{best}^d(t) - x_i^d(t)), & i = 2, \dots, N \end{cases} \quad (\text{Eq 11})$$

$$\alpha = 2e^{n_1 \frac{T-t}{T}} \sin(2\pi n_1) \quad (\text{Eq 12})$$

The maximum number of iterations is denoted as T , α representing the weight constantly and 'n₁' is a random number in between [0, 1].

In this stage, the weight values try to attain the different minimized error values by providing a new search space location. Thus, similar to the chain foraging, the failure of optimal selection of minimal error values may be found in the cyclone approaches.

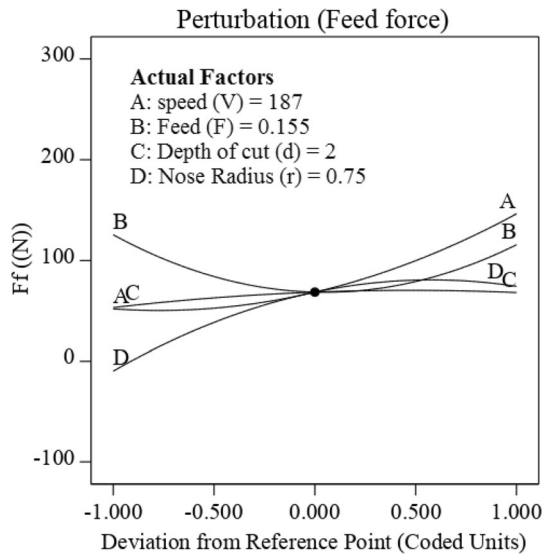


Fig. 6 Perturbation analysis for feed force

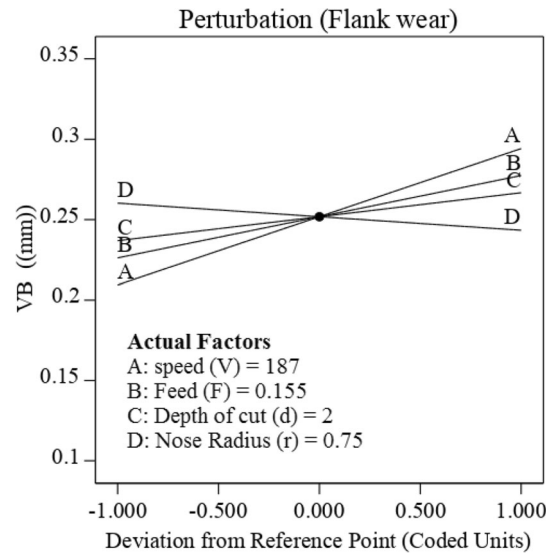


Fig. 8 Perturbation analysis for tool flank wear

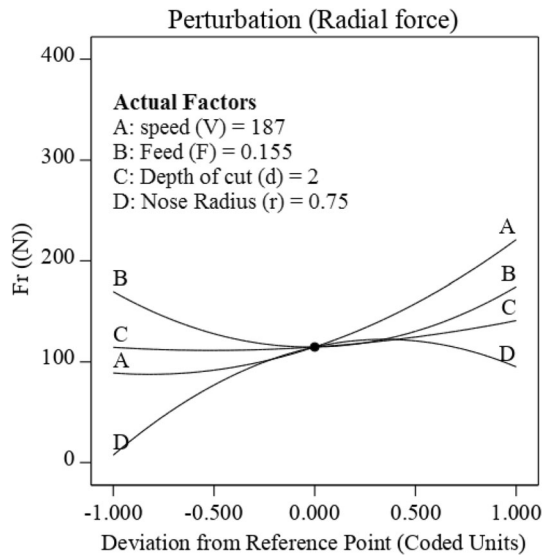


Fig. 7 Perturbation analysis for radial force

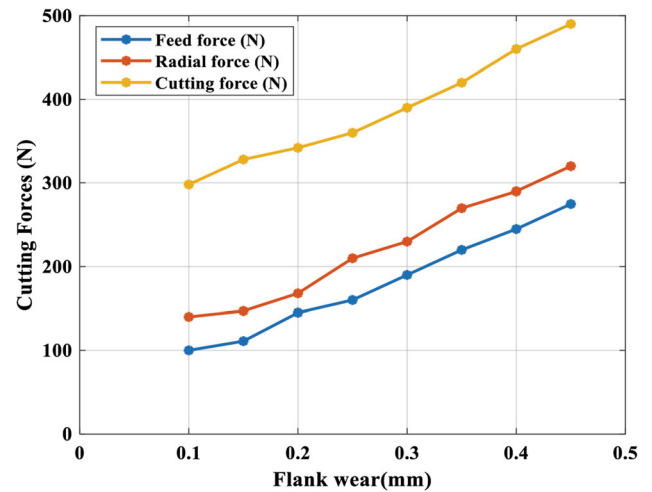


Fig. 9 Effect of tool flank wear on cutting forces

$$x_{rand}^d = LB^d + n(UB^d - LB^d) \quad (\text{Eq 13})$$

$$x_i^d(t+1) = \begin{cases} x_{rand}^d + n(x_{rand}^d - x_i^d(t)) + \alpha(x_{rand}^d - x_i^d(t)), & i = 1 \\ x_{rand}^d + n(x_{i-1}^d(t) + x_i^d(t)) + \alpha(x_{rand}^d - x_i^d(t)), & i = 2, \dots, N \end{cases} \quad (\text{Eq 14})$$

The random position is denoted as x_{rand}^d , LB^d , and UB^d are the lower and the upper limit of the dimensions.

3.1.4 Somersault Foraging. This stage helps to attain the best optimal minimized error value by updating the locations.

$$x_i^d(t+1) = x_i^d(t) + S(n_2 x_{best}^d - n_3 x_i^d(t)), \quad i = 1, \dots, N \quad (\text{Eq 15})$$

The somersault constant is denoted as 'S', 'n₁ and n₂' represent the random number between [0, 1].

4. Result and Discussion

The cutting performances and the cutting force outcomes are tabulated in Table 4.

4.1 Analysis of Forces on Turning Operation

The effect of cutting force majorly depends on the interaction between the workpiece and the tool. In other words, such contacting behavior happens with less time, and more cutting forces are obtained. This is because the plastic deformation of the material is happened because of the increased force in less time. So, the feed and the transverse speed of the tool get increase and contribute to removing material. The feed and speed obtain the linear improvement of Fc. The rubbing force between the tool and the workpiece is called radial force (Ref 41).

The interaction between cutting forces and machining parameters is given in Fig. 5. The interaction of V and F over cutting force is given in Fig. 5(a). In this, the cutting force obeys the speed value of the F. In other words, the cutting force

increase with the increasing in speed and feed rate. Normally, maximum speed value promotes minimum cutting forces due to the minimum chip thickness. In this work, an insufficient cutting temperature makes the workpiece brittle and enhances the tool wear nature. Besides, at increasing speed conditions, maximum temperature occurs, and this suppresses the tool properties. The chip load during machining increases because of the effect of feed rate, which increases cutting force.

The interaction of depth of cut and speed over cutting force is given in Fig. 5(b). In this, the depth of cut is directly proportional to the Fc. When introducing the deeper cuts, more amount of material is removed. Thus the energy dissipation and the requirement of cutting forces tend to improve. In addition, this results in BUE formation. The cutting force analysis by the interaction of feed and nose radius is given in Fig. 5(c). In which the cutting force get increases with the increasing of nose

radius and speed. The interaction between the depth of cut and the feed rate for the Fc is given in Fig. 5(d). In this, the increasing effect of both feed rate and depth of cut tends to increase the cutting force. The overall interactions reveal that the Fc superiorly depends on the speed value than 'F' and 'r'.

The perturbation effect for the feed force by relating the machining input parameters such as feed, depth of cut, and speed is given in Fig. 6. The maximum feed force is obtained by the influence of speed and feed rate than the other machining parameters. Besides, the input parameters 'd' and 'r' get decrease with the increase in feed force. The interrelation of radial force based on machining parameters is given in Fig. 7. In this, the nose radius is indirectly proportional to the feed force. Similar to the feed force analysis, cutting speed gets directly influenced for enhancing the radial forces. The minimal amount of radial force is obtained from the influence of the nose radius. From the experimentation, the obtained optimum radial force is 102.2N, feed force is 155.44N, and cutting force is 102.2N.

4.2 Tool Flank Wear

During machining, tool flank wear is caused because it enhances the chip tool interface temperature, and the tool flank wear is considered a temperature-dependent factor. Besides, it improves the interaction area connecting the tool and the workpiece. The cutting forces are increased due to the machining tool's friction action and wear rate. Thrust force is contributed to the formation of wear rate on the tool because of its rubbing action. At maximum, V and F, the minimal rate of tool wear occurs, resulting in an improvement in tool life and enhanced productivity. Cutting force signals are highly sensitive information carriers on the process's status and are thus the best options for wear monitoring devices. The amount of wear initially depends on the cutting conditions, according to the fraction between the machine's surface and the tool's flank wear. The cutting force is directly proportional to the flank wear. The increasing value of cutting force results failure of the tool. Thus flank wears help in the estimation of tool life.

The perturbation analysis for the flank wear by interrelating input machining parameters is given in Fig. 8. In this, a minimal amount of flank wear is obtained due to the contribution of the nose radius. The input parameter speed

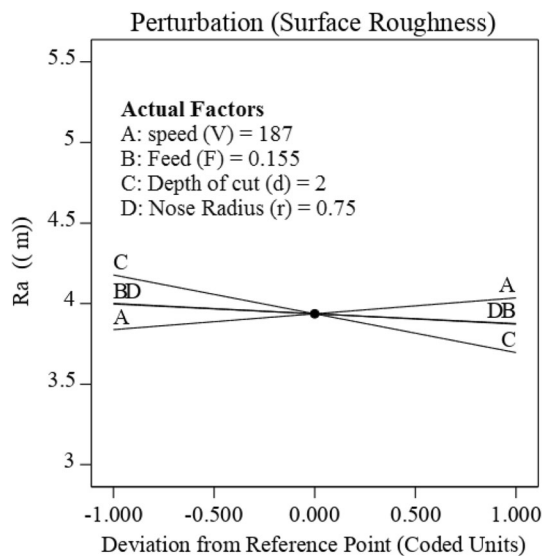


Fig. 10 Influence of input machining conditions on surface roughness

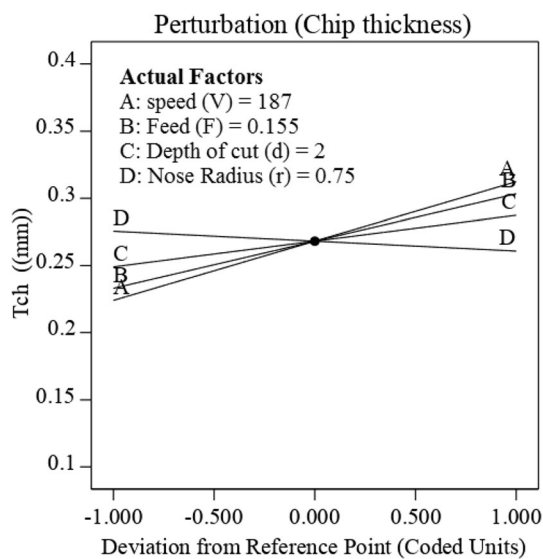


Fig. 11 Perturbation analysis of tool chip thickness

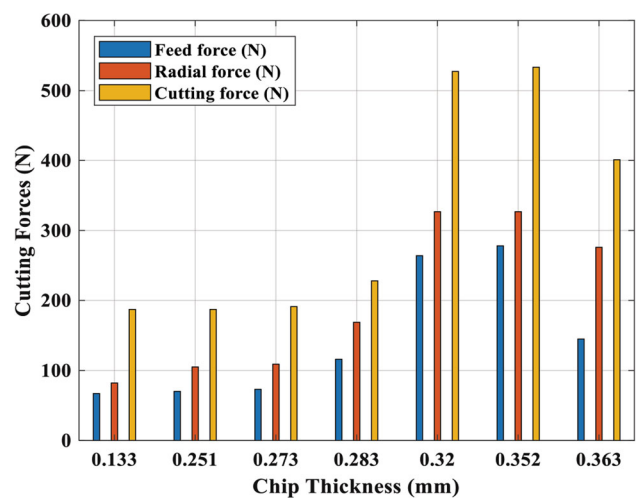


Fig. 12 Effect of tool chip thickness on cutting forces

and feed rate are mainly involved in increasing the level of tool flank wear. Besides, the tool flank wear is just moderately impacted by the depth of cut. The increased rate of tool flank wears results in a moderate level of elastic modulus and stiffness rate. At the beginning of the cutting, the flank wear is null and void. Consequently, the tooltip radius must be increased gradually because of gradual tool wear, and the vibration of the tool will dominate rather than the ideal cutting chatter.

Figure 9 reveals the influences of flank wear over three different cutting forces. Here, the flank wear is minimal at the initial cutting force conditions, and then the flank wear is higher with maximum cutting forces. The minimal VB of 0.1mm is

obtained for the minimal cutting conditions of the radial force, 147N, the feed force is 100N, and the cutting force is 300N.

4.3 Surface Roughness

Surface roughness is measured to analyze the performance of the machined surface. The surface roughness calculation depends on the VB. The life of the tool may be suppressed due to the insufficient quality of the surface. The enhanced behavior of wear increases surface roughness and damages on the tooltip. It is considered an important machining index, and the service life of the machined workpiece is superiorly dependent on the surface roughness. The machined workpiece tends to the presence of microcracks on its surface. Generally, the surface finish is enhanced by using a finishing operation called grinding, and it helps to minimize the abrasive surface defects of the workpiece. During turning, the major causes for the availability of surface roughness are vibration attained in the machining operation, built-up edge formation on the tool, and certain fractures attained in the tip of the tool.

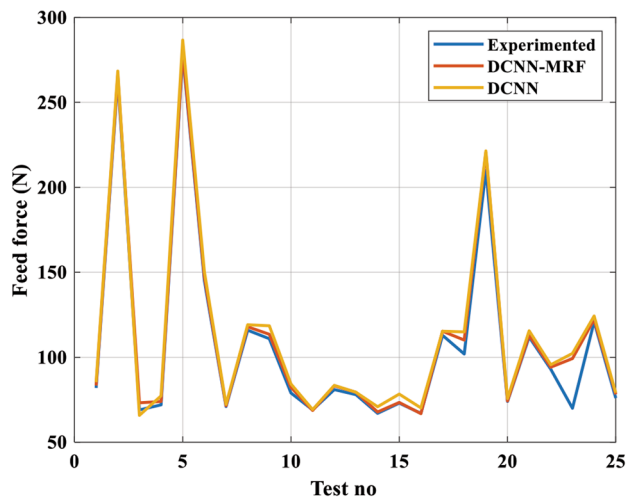
At minimal machining conditions, the obtained surface roughness is $3.105 \mu\text{m}$. By inducing the speed rate, the Ra value increases up to $5.2 \mu\text{m}$. The perturbation effect of machining parameters on the surface roughness is given in Fig. 10. The graph, reveals that the Ra increases with the decrease in the machining parameters except for speed. This is because, at minimal time duration, more machining is possible due to increased speed, which increases Ra and reduces tool life. Besides, surface roughness is unaffected due to the contribution of F and d. Thus, the cutting speed is effectively attained to improve the surface roughness of the workpiece (Ref 16, 17). During increasing feed rates, continuous chip formation happens because of increased speed conditions. This leads to maximizing the temperature level and provides unfavorable surface quality. In this, minimal surface roughness is appeared because of the thermal behavior of tungsten carbide tool material. It can work at elevated temperatures (Ref 23, 24). At maximum nose radius, minimum surface roughness to be achieved, this agrees that in the contact between the workpiece and cutting edge minimum force to be achieved. Surface roughness is at first increased and then decreased to the minimum value, which increases until it reaches a catastrophic failure. The increased feed rate also causes an increment in feed force (Ff) and surface roughness because increasing feed force depends on the feed rate. Besides, surface roughness is more effective with feed force and also cutting tip radius. At a certain point, the Surface roughness increases. Therefore, flank wear changes regularly, and the feed force continuously can be monitored to control Surface roughness.

Table 5 Training and testing parameters

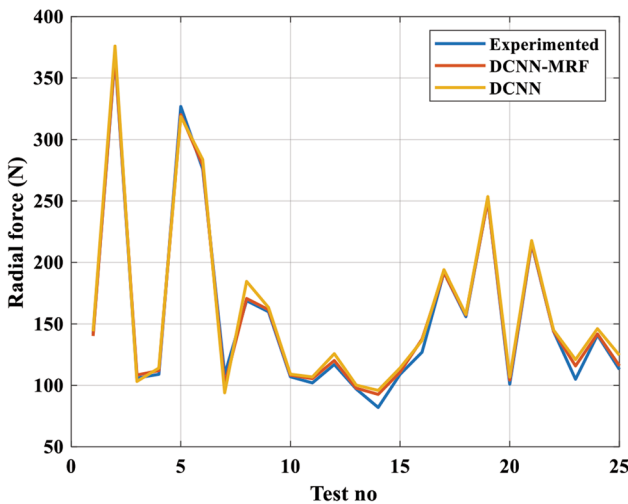
VB, mm		T _{ch} , mm		Ra, μm	
Training	Testing	Training	Testing	Training	Testing
0.297	0.378	0.231	0.265	3.958	4.61
0.30	0.375	0.30	0.37	4.0	4.77
0.251	0.324	0.25	0.312	3.591	3
0.308	0.378	0.340	0.398	3.556	3.98
0.322	0.412	0.350	0.30	3.958	4.55
0.33	0.402	0.368	0.412	4.6717	5.23
0.2565	0.333	0.266	0.302	3.558	4.44
0.28	0.22	0.2862	0.367	3.179	3.75
0.138	0.144	0.151	0.157	3.205	3.88
0.170	0.1788	0.155	0.162	5.411	6.012
0.250	0.31	0.257	0.31	5.15	5.95
0.2978	0.234	0.271	0.32	4.965	4.32
0.236	0.199	0.256	0.199	3.189	3.67
0.161	0.21	0.136	0.144	3.996	4.77
0.253	0.302	0.278	0.331	4.601	5.18
0.215	0.276	0.246	0.302	4.596	5.33
0.256	0.33	0.22	0.287	3.368	3.91
0.148	0.155	0.1796	0.233	3.963	4.59
0.309	0.366	0.362	0.412	3.056	4.23
0.251	0.323	0.2676	0.322	3.958	4.66
0.2274	0.230	0.2566	0.323	3.860	2.95
0.231	0.199	0.273	0.36	3.951	3.25
0.2245	0.220	0.2554	0.201	4.359	3.77
0.230	0.237	0.261	0.20	3.556	2.87
0.2399	0.2477	0.279	0.21	3.565	4.188

Table 6 Regression analysis of different activation function in DCNN

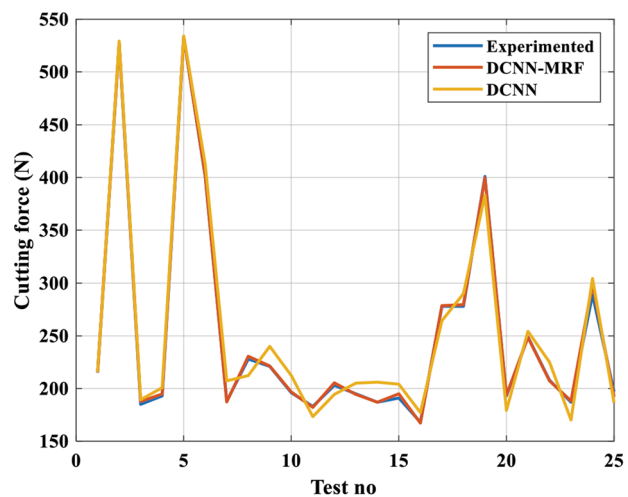
Activation models	Regression			MSE		
	Training	Testing	Validation	Training	Testing	Validation
Random weight+tanh	0.951	0.881	0.9021	1.50	2.37	1.709
MRFO+tanh	0.9845	0.9134	0.942	1.26	1.72	1.562
Random weight+ReLU	0.968	0.887	0.9301	1.47	2.34	1.62
MRFO+ReLU	0.9932	0.923	0.963	1.24	1.68	1.49
Random weight+sigmoid	0.943	0.853	0.899	1.58	2.45	1.78
MRFO+sigmoid	0.9812	0.896	0.931	1.32	2.16	1.61



(a) Feed Force-Prediction



(b) Radial Force-Prediction



(c) Cutting Force-Prediction

Fig. 13 Predicted outcomes for cutting forces

4.4 Tool Chip Thickness

The energy efficiency of the machining system is analyzed based on the thickness of the chip. During turning, the energy consumption get increases for the maximum thickness of the chip. In other words, less amount of energy is required for the minimum chip thickness. Besides, the chip thickness has a supreme effect on cutting forces. The tool-workpiece interfacial temperature gets enhanced when higher the cutting speed, which reduces the cutting forces and minimizes the thickness of the chip. This action results in minimizing the shear strength of the workpiece.

The thickness of the equivalent chip is increased with an increase in the depth of cut and cutting speed. The tool chip's contact area is increased with an increase in the value of the depth of the cut; hence, tool chip thickness is increased. The higher temperature is produced at maximum cutting speed, which leads to rapid tool wear. Because of the produced higher temperature, the manufactured chip also has a high temperature. The thickness of the chip is increased due to the adhesion of the tool. The tool material's adhesion leads the tool material to place over the back chip's surface at high temperatures. It decreased the depth of cut and increased the speed of the cut resulted in maximum vertical force.

Figure 11 demonstrates the perturbation effect of chip thickness based on machining parameters. In this, the chip thickness increases with the decreasing in nose radius and increases with the remaining machining performances. At the rate of speed 187 m/min, the maximum amount of chip thickness is obtained.

The relationship between chip thickness and cutting forces is given in Fig. 12. In this, the cutting force is optimal than the radial and the feed force. The thickness of the chip gets increases due to the influence of cutting force enhancement. The chip with the maximum thickness of 0.352mm is obtained due to the maximum cutting forces such as 278 N of Feed force, 327N of radial force, and 533 N cutting force.

4.5 Prediction by Hybrid DCNN Based MRFO:

After analyzing the experimental outcomes, the prediction behavior is achieved using Hybrid DCNN Based MRFO. In this, the hybridization activity helps to optimize the superior weight values from the neural network. Normally, in Neural networks, the prediction activity is done by training the actual values with random weight values. Such randomized activity is suppressed using Manta-Ray Foraging Optimizer. The random selection of weight values may be missed to promote accurate prediction due to error. The training and the testing parameters are given in Table 5.

The regression analysis of DCNN with different activation functions is given in Table 6. In which, MRFO based optimized weight contributed DCNN promotes superior regression percentage with minimal error than the random weight functions. In RSM, the obtained R^2 values are in the ranges of 0.91 to 0.962. In the view of activation functions, ReLU promotes better performances than the rest of the functions, namely tanh and sigmoid. ReLU conveniently helps to backpropagation of errors and enhance the convergence rate.

The predicted outcomes when using ReLU-based activation functions are given in Fig. 13 and 14. Figure 13 explains the predicted values of the cutting forces by using hybrid DCNN-MRFO and non-hybrid DCNN. In this, the predicted outcomes

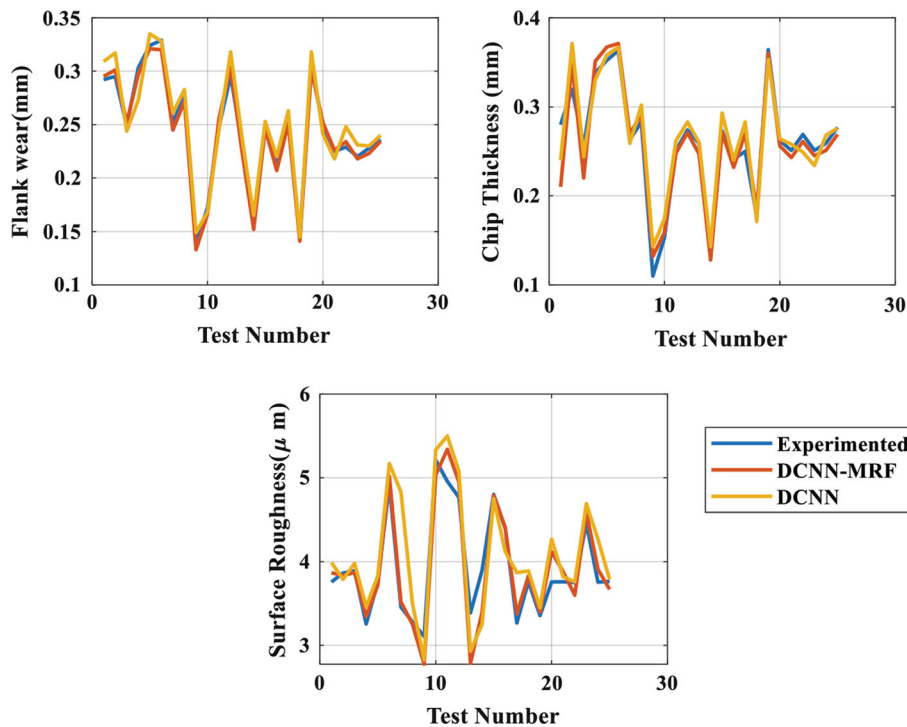


Fig. 14 Predicted outcomes of flank wear, chip thickness, and surface roughness

are nearly closer to the experimented outcomes of cutting force. Compared with the non-hybrid DCNN, the variations attained between the experimented and the proposed hybrid DCNN-based MRFO are lesser. So, we conclude that our proposed DCNN-based MRFO promotes better and accurate predicted values than the non-hybrid prediction model. The optimized weight values are selected using hybrid DCNN-MRFO and are used to provide an accurate prediction. The prediction analysis for the machining performances is demonstrated in Fig. 14. The prediction results for the minimal flank wear using DCNN-MRFO is 0.133 mm, and DCNN is 0.149 mm. The DCNN-MRFO based predicted surface roughness is 2.778 and 3.678 μ m.

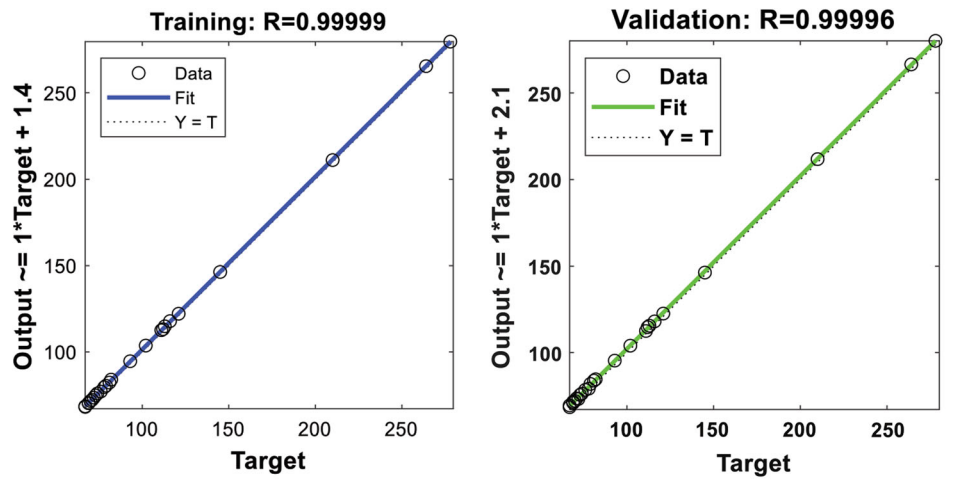
The correlation analysis of experimented and the hybrid DCNN-based MRFO-based predicted outcomes for cutting forces are given in Fig. 15. Figure 16 explains the fitness analysis of machining performances are flank wear, chip thickness, and surface roughness. The target values are more fitted to the experimented values in both the training and the validation analysis. Thus errors obtained from the hybrid DCNN-based MRFO are less than the non-hybrid DCNN.

The Root Mean Square Error (RMSE) analysis of hybrid and non-hybrid prediction models is compared in Fig. 17. In the view of cutting forces, the obtained error values for the hybrid DCNN-based MRFO are in the range of 0.17 to 0.48. When using DCNN with random weights, the error values range from 0.4 to 0.68. During DCNN-MRFO prediction, the obtained RMSE for the flank wear, chip thickness, and surface roughness are 0.003, 0.005, and 0.006. Besides, the RMSE obtained from the non-hybrid DCNN is 0.008, 0.012, and 0.085. The results proved that the errors are more random than the MRFO-based optimum weights during prediction. This is because in MRFO based optimization the weight values are selected closer to the target.

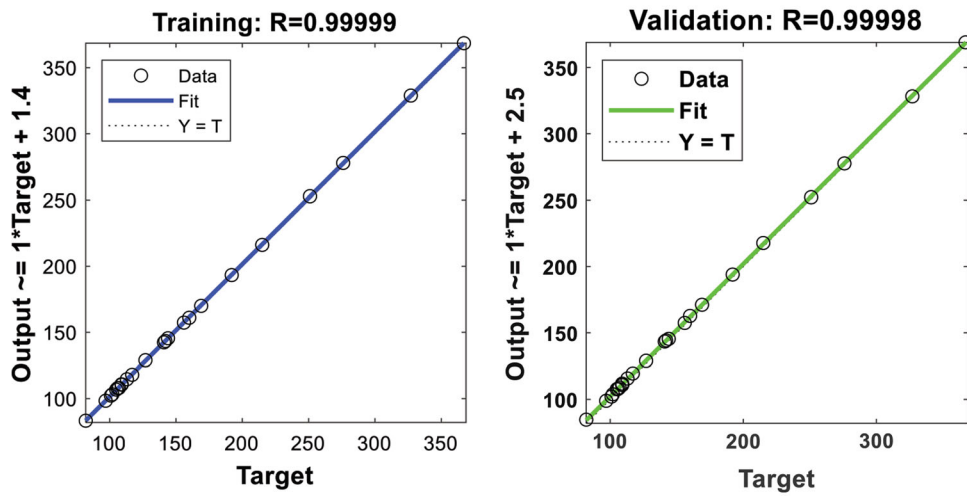
5. Conclusion

The mild steel turning with a tungsten carbide tool is conducted in this research work. The turning operation is performed by varying the input parameters such as V , d , F , and r . The different cutting forces, VB , Ra , and Tch , are analyzed and predicted with the help of DCNN based Manta-Ray Foraging optimization. The effect of cutting forces on VB and tool chip thickness is also analyzed in this study.

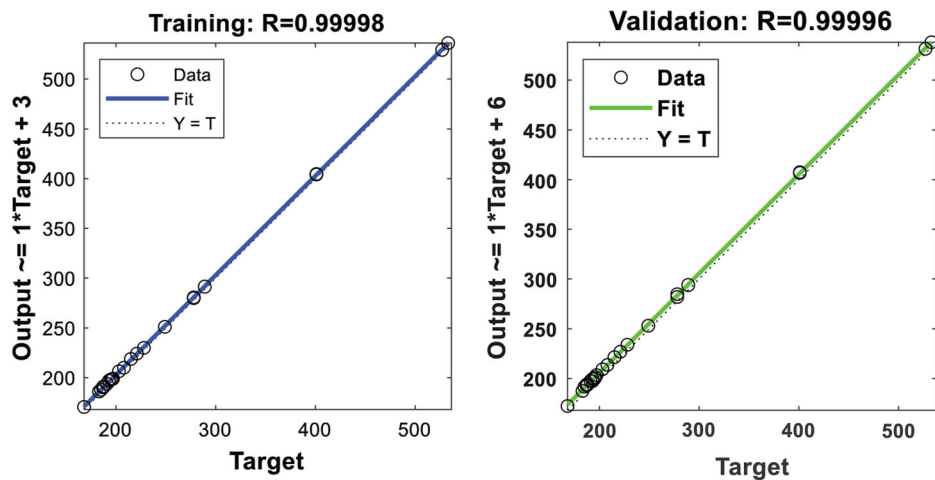
- The maximum amount of obtained feed force is 67N, cutting force is 82N, and radial force is 187 N. The cutting speed is more effectively influences the radial, feed, and cutting forces. At minimal machining conditions, DCNN-MRFO based predicted radial, cutting force, feed forces are 67.23, 82.3, and 186.21N.
- In the tool flank wear analysis, the nose radius helps to minimize the tool wear. Besides, the wear rate tends to be maximum because of the contribution of cutting speed. The obtained minimal tool flank wear is 0.139mm. In the view of cutting forces, the contribution of feed force promotes less amount of wear. The prediction results from DCNN-MRFO are 0.133 mm, and DCNN is 0.149mm.
- In the view of Ra , resistance to surface roughness is maximized due to the effect of depth of cut. Similar to VB analysis, the effect of cutting speed superiorly contributes to enhancing the workpiece's surface roughness. From the overall experimentation, the gained minimal surface roughness is 3.105 μ m. The DCNN-MRFO based predicted surface roughness is 2.778 and 3.678 μ m.
- The chip thickness gets improved due to the speed, and its effect is minimized because of the nose radius. Besides, Tch is increased with the increasing of cutting forces. The obtained chip thickness is in the ranges of



(a) Feed Force

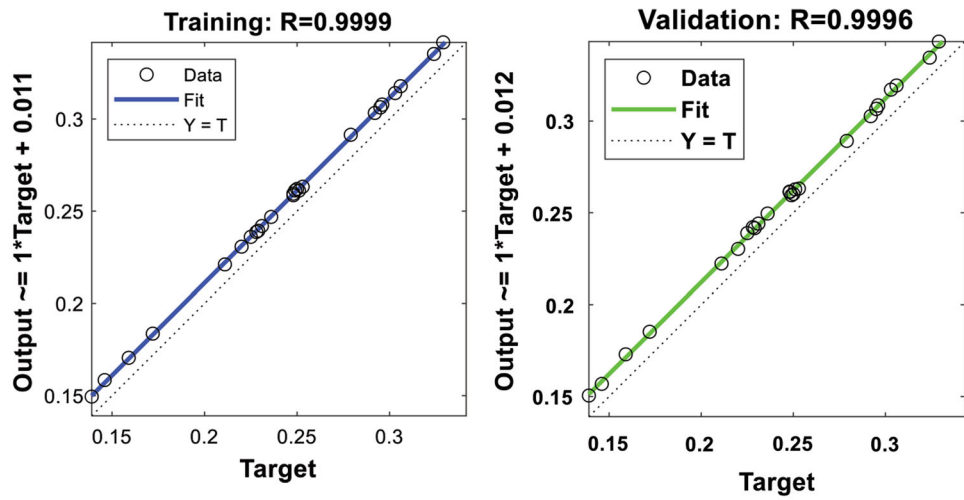


(b) Radial Force

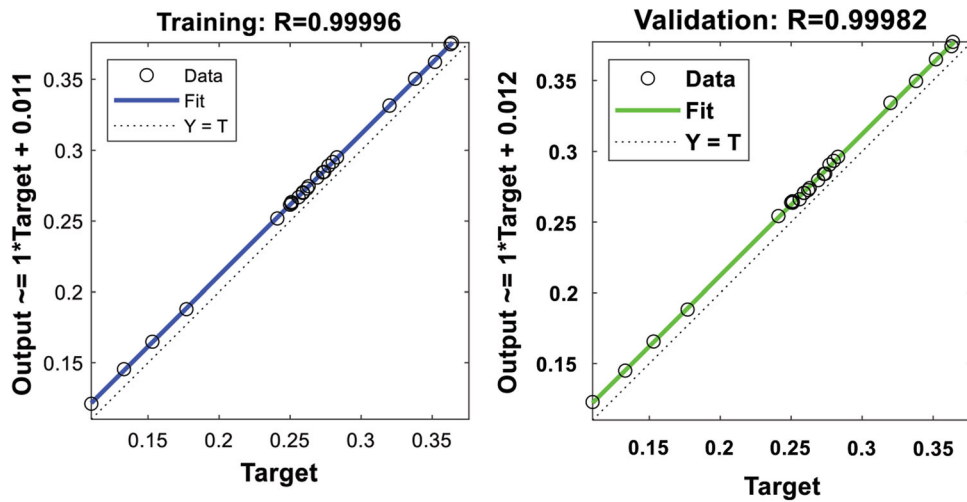


(c) Cutting force

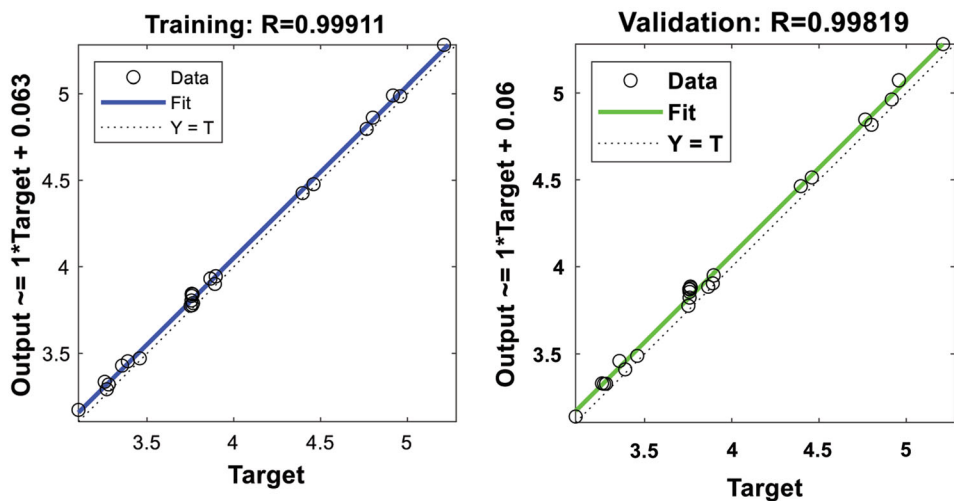
Fig. 15 Regression plots for cutting forces



(a) Flank wear



(b) Tool chip thickness



(c) Surface roughness

Fig. 16 Regression plots for machining performances

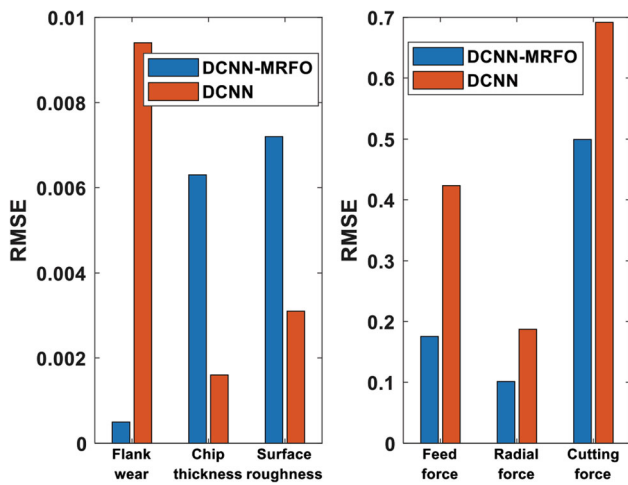


Fig. 17 Error analysis of machining outcomes

0.11 to 0.363 mm. The prediction results from DCNN-MRFO are 0.132 mm, and DCNN is 0.143 mm.

- The root mean error range observed for the hybrid DCNN-MRFO is 0.0005 to 0.06, and the non-hybrid DCNN is 0.16 to 0.5.

From the overall analysis, it concludes that the cutting speed is involved in affecting the machining conditions. Our proposed hybrid DCNN -MRFO predicted outcomes are nearly closer to the experimented outcomes than the DCNN predicted results.

Funding

No funding is provided for the preparation of the manuscript.

Data Availability

Data sharing not applicable to this article as no datasets were generated or analyzed during the current study.

Conflict of interest

Authors *¹Thangavel Palaniappan, ²Prakasam Subramaniam declared that they have no conflict of interest.

Ethical Standards

This article does not contain any studies with human participants or animals performed by any of the authors.

Consent to Participate

All the authors involved have agreed to participate in this submitted article.

Consent for Publication

All the authors involved in this manuscript give full consent for publication of this submitted article.

References

1. H. Aouici, M.A. Yaltese, B. Fnides and K. Chaoui, Modelling Optimization of Hard Turning of x38CrMoV5-1 Steel with CBN Tool Machining Parameters Effects on Flank Wear and Surface Roughness, *J. Mech. Sci. Technol.*, 2011, **25**(11), p 2843–2851.

2. S. Kumar, and B. Singh, A New Approach to Explore Tool Chatter in Turning Operation on the Lathe. *Australian J. Mech. Eng.* 1–20 (2019)
3. S. Dinesh, V. Vijayan, A. Parthiban, C. Saravanan, and B.S. Kumar, Modeling and optimization of machining parameters for turning of mild steel using single-point cutting tool made of P20 tool steel, In *Advances in Industrial Automation and Smart Manufacturing*. Springer, Singapore, 2021, p. 285–295
4. M. Rafiqhi, M. Özdemir, S. Al Shehaby, et al., Sustainable Hard Turning of High Chromium AISI D2 Tool Steel Using CBN and Ceramic Inserts. *Trans. Indian Inst. Met.* 2021, **74**, p 1639–1653
5. J. Rajaparthiban, M. Ravichandran, B. Stalin, P.R. Kumar and V. Mohanavel, Machining of EN31 Steel Using Carbide Insert–A Statistical Approach, *Materials Today: Proceedings*, 2020, **22**, p 2559–2564.
6. K. Arunkarthikeyan and K. Balamurugan, Experimental studies on deep cryo treated plus tempered tungsten carbide inserts in turning operation. In *Advances in industrial automation and smart manufacturing*. Springer, Singapore, 2021. 313–323
7. A. Das, M. Kamal, S.R. Das, S.K. Patel, A. Panda, M. Rafiqhi and B.B. Biswal, Comparative assessment between AlTiN and AlTiSiN coated carbide tools towards machinability improvement of AISI D6 steel in dry hard turning. *Proceedings of the Institution of Mechanical Engineers, Part C: Journal of Mechanical Engineering Science*, 2021, p.09544062211037373
8. M.E. Korkmaz, N. Yaşar and M. Günay, Numerical and Experimental Investigation of Cutting Forces in Turning of Nimonic 80A Superalloy, *Eng. Sci. Technol. Int. J.*, 2020, **23**(3), p 664–673
9. L.B. Abhang and M. Hameedullah, Modeling and analysis of tool wear based on cutting force and chip-tool interface temperatures in turning, *Advanced manufacturing and materials science*. Springer, Cham, 2018, p 411–420
10. I.P. Okokpujie, O.S. Ohunakin, C.A. Bolu and K.O. Okokpujie, Experimental Data-Set for Prediction of Tool Wear During Turning of Al-1061 Alloy by High Speed Steel Cutting Tools, *Data Brief*, 2018, **18**, p 1196–1203.
11. A.B. Bijithmon and N.G. Smitha, Optimization of Surface Roughness of EN24T Steel Using Genetic Algorithm in Turning Operation, *Int. J. Eng. Res. Technol.*, 2017, **6**(5), p 504–510.
12. N.C. Ghuge and A.M. Mahalle, Experimental Investigation on the Performance of Soyabean Oil and Blassocut-4000 During Turning of AISI in Terms of Cutting Forces, *Int. J. Scientific Res. Sci. Eng. Technol. (IJSRSET)*, 2016, **2**(3), p 330–333.
13. Z. Zhu, S. To, W.L. Zhu, P. Huang and X. Zhou, Cutting Forces in Fast-/Slow Tool Servo Diamond Turning of Micro-Structured Surfaces, *Int. J. Mach. Tools Manuf.*, 2019, **136**, p 62–75.
14. Y. Wei, M.R. Kim, D.W. Lee, C. Park and S.S. Park, Effects of Micro Textured Sapphire Tool Regarding Cutting Forces in Turning Operations, *Int. J. Precis.Eng. Manuf. Green Technol.*, 2017, **4**(2), p 141–147.
15. M. Dumas, G. Kermouche, F. Valiorgue, A.V. Robaey, F. Lefebvre, A. Brosse, H. Karaoui and J. Rech, Turning-Induced Surface Integrity for a Fillet Radius in a 316L Austenitic Stainless Steel, *J. Manuf. Process.*, 2021, **68**, p 222–230.
16. R.A. Laghari, J. Li, Z. Xie and S.Q. Wang, Modeling and Optimization of Tool Wear and Surface Roughness in Turning of Al/Sicp Using Response Surface Methodology, *3D Res.*, 2018, **9**(4), p 46.
17. M.D. Selvam, P. Senthil and N.M. Sivaram, Parametric Optimization for Surface Roughness of AISI 4340 Steel During Turning Under Near Dry Machining Condition, *Int. J. Mach. Mach. Mater.*, 2017, **19**(6), p 554–569.
18. S.S. Babu and B.K. Vinayagam, Surface Roughness Prediction Model Using Adaptive Particle Swarm Optimization (APSO) Algorithm, *J. Intell. Fuzzy Syst.*, 2015, **28**(1), p 345–360.
19. A. Şahinoğlu and M. Rafiqhi, Investigation of Vibration, Sound Intensity, Machine Current and Surface Roughness Values of AISI 4140 During Machining on the Lathe, *Arab J Sci Eng.* 2020, **45**, p 765–778.
20. S. Atla and M.S. Surya, Influence of Cutting Fluids on Tool Wear and Surface Roughness During Turning of Aisi 316 Austenitic Stainless Steel, *IJERT*, 2017, **6**(07), p 112–115
21. M. Mia and N.R. Dhar, Optimization of Surface Roughness and Cutting Temperature in Highpressure Coolant-Assisted Hard Turning Using Taguchi Method, *Int. J. Adv. Manuf. Technol.*, 2017, **88**(1–4), p 739–753.

22. A. Şahinoğlu and M. Rafighi, Optimization of Cutting Parameters with Respect to Roughness for Machining of Hardened AISI 1040 Steel, *Mater. Test.*, 2020, **62**(1), p 85–95.
23. F. Bayraktar and F. Kara, Investigation of the Effect on Surface Roughness of Cryogenic Process Applied to Cutting Tool, *Int. J. Anal. Exp. Finite Element Anal.*, 2020, **7**(2), p 19–27.
24. A. Das, S.K. Patel, B.B. Biswal, N. Sahoo and A. Pradhan, Performance Evaluation of Various Cutting Fluids Using MQL Technique in Hard Turning of AISI 4340 Alloy Steel, *Measurement*, 2020, **150**, p 107079.
25. A.A. Selaimia, H. Bensouilah, M.A. Yallese and I.K. Meddour, Modeling and optimization in Dry Face Milling of X2CrNi18-9 Austenitic Stainless Steel Using RMS and Desirability Approach, *Measurement*, 2017, **107**, p 53–67.
26. F. Kara, Optimization of Cutting Parameters in Finishing Milling of Hardox 400 Steel, *Int. J. Anal. Exp. Finite Element Anal.*, 2018, **5**(3), p 44–49.
27. B.S. Prasad and M.P. Babu, Correlation Between Vibration Amplitude and Tool Wear in Turning: Numerical and Experimental Analysis, *Eng. Sci. Technol. Int. J.*, 2017, **20**(1), p 197–211.
28. D.S.C. Kishore, K.P. Rao and A. Mahamani, Investigation of Cutting Force, Surface Roughness and Flank Wear in Turning of In-situ Al6061-TiC Metal Matrix Composite, *Procedia Mater. Sci.*, 2014, **6**, p 1040–1050.
29. M. Kuntoğlu and H. Sağlam, Investigation of Progressive Tool Wear for Determining of Optimized Machining Parameters in Turning, *Measurement*, 2019, **140**, p 427–436.
30. D. Manivel and R. Gandhinathan, Optimization of Surface Roughness and Tool Wear in Hard Turning of Austempered Ductile Iron (Grade 3) Using Taguchi Method, *Measurement*, 2016, **93**, p 108–116.
31. M. Mia, P.R. Dey, M.S. Hossain, M.T. Arafat, M. Asaduzzaman, M.S. Ullah and S.T. Zobaer, Taguchi S/N Based Optimization of Machining Parameters for Surface Roughness, Tool Wear and Material Removal Rate in Hard Turning Under MQL Cutting Condition, *Measurement*, 2018, **122**, p 380–391.
32. E.O. Ezugwua, D.A. Fadera, J. Bonneya, R.B. Da Silva and W.F. Salesa, Modelling the Correlation between Cutting and Process Parameters in High Speed Machining of Inconel 718 Alloy Using an Artificial Neural Network, *Int. J. Mach. Tools Manuf.*, 2005, **45**, p 1375–1385.
33. J. Senveter, S. Klancnik, J. Balic and F. Cus, Prediction of Surface Roughness Using A Feed-Forward Neural Network, *Manag. Prod. Eng. Rev.*, 2010, **1**(2), p 47–55.
34. T. Sk and S. Shankar, Tool wear prediction in hard turning of EN8 steel using cutting force and surface roughness with artificial neural network, *Proc. Inst. Mech. Eng. C J. Mech. Eng. Sci.*, 2020, **234**(1), p 329–342.
35. A. Salimi, A. Erdem and M. Rafighi, Applying a Multi Sensor System to Predict and Simulate the Tool Wear Using of Artificial Neural Networks, *Scientia Iranica*, 2017, **24**(6), p 2864–2874.
36. S.O. Sada, Improving the Predictive Accuracy of Artificial Neural Network (ANN) Approach in a Mild Steel Turning Operation, *Int. J. Adv. Manuf. Technol.*, 2021, **112**, p 2389–2398
37. G.S. Babu, P. Zhao and X.L. Li, Deep convolutional neural network based regression approach for estimation of remaining useful life, In International conference on database systems for advanced applications Springer, Cham. 2016 April, p 214–228
38. Ö. Erkan, B. Işık, A. Çiçek and F. Kara, Prediction of Damage Factor in End Milling of Glass Fibre Reinforced Plastic Composites Using Artificial Neural Network, *Appl. Compos. Mater.*, 2013, **20**(4), p 517–536.
39. W. Zhao, Z. Zhang and L. Wang, Manta Ray Foraging Optimization: An Effective Bio-Inspired Optimizer for Engineering Applications, *Eng. Appl. Artif. Intell.*, 2020, **87**, p 103300.
40. B. Sheng, T. Pan, Y. Luo and K. Jermsittiparsert, System Identification of the PEMFCs based on Balanced Manta-Ray Foraging Optimization algorithm, *Energy Rep.*, 2020, **6**, p 2887–2896.
41. F. Kara, K. Aslantas and A. Çiçek, ANN and Multiple Regression Method-Based Modelling of Cutting Forces in Orthogonal Machining of AISI 316L Stainless Steel, *Neural Comput. Appl.*, 2015, **26**(1), p 237–250.

Publisher's Note Springer Nature remains neutral with regard to jurisdictional claims in published maps and institutional affiliations.